Zero-Shot Anomaly Detection without Foundation Models

Aodong Li*1 Chen Qiu*2 Marius Kloft Padhraic Smyth Maja Rudolph†2 Stephan Mandt†1

Abstract

Anomaly detection (AD) tries to identify data instances that deviate from the norm in a given data set. Since data distributions are subject to distribution shifts, our concept of "normality" may also drift, raising the need for zero-shot adaptation approaches for anomaly detection. However, the fact that current zero-shot AD methods rely on foundation models that are restricted in their domain (natural language and natural images), are costly, and oftentimes proprietary, asks for alternative approaches. In this paper, we propose a simple and highly effective zero-shot AD approach compatible with a variety of established AD methods. Our solution relies on training an off-theshelf anomaly detector (such as a deep SVDD) on a set of inter-related data distributions in combination with batch normalization. This simple recipe-batch normalization plus meta-training-is a highly effective and versatile tool. Our results demonstrate the first zero-shot anomaly detection results for tabular data and SOTA zero-shot AD results for image data from specialized domains.

1. Introduction

Anomaly detection (AD)—the task of identifying data instances deviating from the norm (Ruff et al., 2021)—is significant in many application domains, ranging from fake review identification and bot detection in social networks to tumor recognition and industrial fault detection. AD is especially important in safety-critical applications: failing to recognize anomalies in a chemical plant or a self-driving car may put lives at stake.

The notion of an "anomaly" inherently depends on our no-

tion of "normal" data. However, the notion of normality depends on the context, and in particular, what we consider normal may drift over time. For example, when monitoring network traffic for intrusions, normal data may differ from user to user and day to day. Medical imaging data depends on the patient and the laboratory equipment employed.

Adapting an anomaly detector to drift in the normal data distribution is the task in *zero-shot AD* (Liznerski et al., 2022; Esmaeilpour et al., 2022; Schwartz et al., 2022). To date, zero-shot AD has primarily been dealt with by using *foundation models*—large neural networks trained on massive unlabeled data at scale by self-supervised learning (Radford et al., 2021; He et al., 2022).

Foundation models have proven impactful in many areas, especially in vision and NLP (Radford et al., 2021; Brown et al., 2020; Yu et al., 2022). However, many AD applications involve data from specialized domains, such as data from industrial fault detection, network intrusion detection, bot detection, healthcare, medical imaging, and other applications. Besides text and images, AD commonly involves time series and tabular data for which no foundation models are currently available. Furthermore, foundation models have a large carbon footprint and are currently owned by a few major companies, raising questions about their free availability to the broader public.

This paper challenges the common assumption that one needs foundation models for zero-shot AD. The main contribution of this paper is Adaptive Centered Representations (ACR), a new lightweight model for zero-shot AD. ACR is theoretically grounded, simple, domain-independent, and easy to implement and use. It can be employed for zero-shot AD using data from any domain, whether it is time series or tabular data, DNA sequences, or graphs.

ACR relies on a simple idea, namely, training an anomaly detector on a meta-set of related data distributions using batch normalization layers. In this paper, we will show that this simple modification to the existing training paradigm will allow the model to automatically adapt to data from new but related distributions, i.e., do zero-shot learning. This approach applies to a variety of backbone models commonly used in deep AD (Ruff et al., 2018; Qiu et al., 2021).

We exemplify our approach using the DSVDD model for

^{*}Equal contribution †Joint supervision ¹Department of Computer Science, University of California, Irvine, USA ²Bosch Center for Artificial Intelligence, Pittsburgh, USA ³Department of Computer Science, TU Kaiserslautern, Germany. Correspondence to: Aodong Li <aodongl1@uci.edu>, Maja Rudolph < Maja.Rudolph@us.bosch.com>, Stephan Mandt < mandt@uci.edu>.

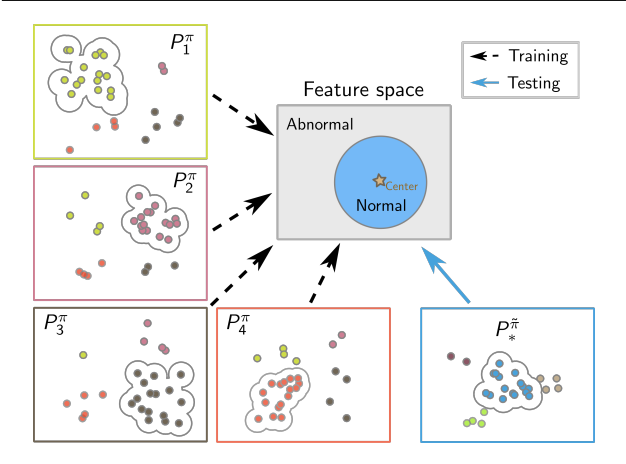


Figure 1. Illustration of training (black) and testing (blue) exemplified for DSVDD. During training, the model learns to solve all tasks jointly, a) learning separable features for samples from different distributions and b) learning to map the samples from the major (normal) distribution to a shared learned center in embedding space while mapping other samples away from the center. At test time, the learned model exploits the learned inductive bias to map the normal (majority) samples to the center of embedding space while mapping anomalous samples away from the center.

AD. DSVDD is trained to map high-dimensional data, such as images, to a single point (called "the center") in a lower-dimensional feature space. At test time, DSVDD scores anomalies based on their ℓ_2 distance to the center, i.e., distant points are considered anomalies.

Fig. 1 illustrates our training and testing setups for DSVDD. Here, we observe four related datasets for training, each one equipped with abnormal (scattered) and normal samples (clustered and encircled). We train a single DSVDD, using batch normalization, to map normal samples into the vicinity of a center in a feature space (blue region)¹. For a new dataset (blue frame), our method will instantaneously adapt to the new data distribution and map all normal samples to the same blue region in the feature space.

Why does this method work? Batch normalization is a mechanism to re-calibrate the distribution of intermediate features in a mini-batch based on the *majority* of data in the batch. Since we assume that this majority will be representative of each data distribution's "normal" component, we can train a single one-class AD model on multiple data distributions (with relative distribution shifts) simultaneously.

Our contributions can be summarized as follows:

 A simple but effective new method. Our results for the first time show that training off-the-shelf deep anomaly detectors on a meta-training set, using batch normalization layers, gives automatic zero-shot generalization for AD.

- Zero-shot AD on tabular data. To the best of our knowledge, we provide the first results for zero-shot AD results on tabular data. We show that our adaptation approach retains a high degree of accuracy.
- Competitive results for images. Our results show that
 we achieve state-of-the-art zero-shot AD results on nonnatural images and competitive results on natural images.

2. Related Work

Deep AD. Many recent advances in AD built on deep learning methods (Ruff et al., 2021). One early strategy was to use autoencoder- (Principi et al., 2017; Zhou & Paffenroth, 2017; Chen & Konukoglu, 2018) or density-based (Schlegl et al., 2017; Deecke et al., 2018) models. Another pioneering stream of research combines one-class classification (Schölkopf et al., 2001) with deep learning (Ruff et al., 2018; Qiu et al., 2022a). Many other approaches to deep AD are self-supervised. They employ a self-supervised loss function to train the detector and score anomalies (Golan & El-Yaniv, 2018; Hendrycks et al., 2019; Sohn et al., 2020; Bergman & Hoshen, 2020; Qiu et al., 2021; Schneider et al., 2022; Shenkar & Wolf, 2021).

All these approaches assume that the data distribution will not change too much at test time. However, in many practical scenarios, there will be significant shifts in the abnormal distribution and even the normal distribution. For example, Dragoi et al. (2022) observed that existing AD methods fail in detecting anomalies when distribution shifts occur in network intrusion detection.

Few-shot AD. Several recent works have studied adapting an anomaly detector to shifts by fine-tuning on a few test samples. One stream of research applies model-agnostic meta learning (MAML) (Finn et al., 2017) to various deep AD models, including one-class classification (Frikha et al., 2021), generative adversarial networks (Lu et al., 2020), autoencoder (Wu et al., 2021), graph deviation networks (Ding et al., 2021), and supervised classifiers (Zhang et al., 2020; Feng et al., 2021). Some approaches extend prototypical networks to few-shot AD (Kruspe, 2019; Chen et al., 2022). Kozerawski & Turk (2018) learn a linear SVM with a few samples on top of a frozen pre-trained feature extractor, while Sheynin et al. (2021) learn a hierarchical generative model from a few normal samples for image AD. Wang et al. (2022) learn an energy model for AD. The anomalies are scored by the error of reconstructing their embeddings from a set of normal features that are adapted with a few test samples.

In contrast to all few-shot AD methods, we propose a zeroshot AD method and demonstrate that the learned AD model can adapt itself to new tasks without any support samples.

¹ and map abnormal samples away from the center where applicable.

Zero-shot AD. Foundation models pre-trained on massive training samples have achieved remarkable results on zero-shot tasks on images (Radford et al., 2021; Yu et al., 2022; Jia et al., 2021; Yuan et al., 2021). For example, contrastive language-image pre-training (CLIP) (Radford et al., 2021) is a pre-trained language-vision model learned by aligning images and their paired text descriptions. One can achieve zero-shot image classification with CLIP by searching for the best-aligned text description of the test images. Esmaeilpour et al. (2022) extend CLIP with a learnable text description generator for out-of-distribution detection. Liznerski et al. (2022) apply CLIP for zero-shot AD and score the anomalies by comparing the alignment of test images with the correct text description of normal samples. Schwartz et al. (2022) study the performance of masked autoencoder (He et al., 2022), a pre-trained vision foundation model, on few-shot and zero-shot image AD using the reconstruction error as the anomaly score.

However, foundation models are not available for all data types. Foundation models do not exist for, e.g., tabular data, the arguably most general and flexible data type and significant in applications such as network security and industrial fault detection. Also, existing adaptations of foundation models for AD (e.g., CLIP) may generalize poorly to specific domains that have not been covered in their massive training samples. For example, Liznerski et al. (2022) observed that CLIP performs poorly on non-natural images, such as MNIST digits. In contrast, ACR does not rely on a powerful pre-trained foundation model, enabling zero-shot AD on various data types.

3. Method

We begin by describing our problem statement in Sec. 3.1 and then present our proposed solution in Sec. 3.2. Finally, we discuss an important extension of our method that leads to improved performance in Sec. 3.3.

3.1. Problem Statement

We consider a distribution of interrelated data distributions, a standard assumption in meta-learning and zero-shot learning (Baxter, 2000). Let $\mathcal Q$ be a (meta-)distribution from which we sample K training distributions P_1, \ldots, P_K and a test distribution P_* :

$$P_1, \dots, P_K, P_* \stackrel{\text{i.i.d.}}{\sim} \mathcal{Q}.$$
 (1)

We assume that the distributions in \mathcal{Q} share some common structure, such that training a model on one distribution has the potential to aid in deploying the model on another distribution. For example, the data \mathbf{x} could be radiology images from patients, and each P_j or P_* could be a distribution of images from a specific hospital. These distributions share similarities but differ systematically because of dif-

ferences in radiology equipment, calibration, and patient demographics.

Our goal is to use data from only the distributions $P_1, ..., P_K$ to learn an *anomaly detector*, i.e., a model that learns to distinguish samples compatible with P_j from samples not coming from P_j (see details below).

After training, we expect our anomaly detector to *instantly* adapt (in a zero-shot fashion) to the test distribution P_* without further training, i.e., discover anomalies with respect to the "new normal" distribution P_* . Details on how to accomplish this goal will be described next.

3.2. Adaptively Centered Representations

As common in AD, we propose to learn an *anomaly score* function $S_{\theta}(\mathbf{x}|P)$, characterized by learnable parameters θ and a distribution $P \in \{P_*, P_1, \dots, P_K\}$ such that

$$S_{\theta}(\mathbf{x}|P) \to \begin{cases} \text{small} & \text{if } \mathbf{x} \sim P \\ \text{large} & \text{if } \mathbf{x} \not \sim P \end{cases}$$
 (2)

At training, the parameters θ are learned to satisfy Eq. (2) with $P = P_j$ on samples x from the training distributions P_1, \ldots, P_K . Since the training and test distribution(s) are drawn from the same meta distribution (Eq. (1)), the test distribution $P = P_*$ should approximately satisfy Eq. (2) too, if K is sufficiently large. In other words, $S_{\theta}(\mathbf{x}|P_*)$ is a reasonable anomaly score at test time.

In any practical training or testing environment, we encounter a mixture of normal samples and anomalies. To simulate the fact that each P_j during training is not "pure", we contaminate it by admixing a fraction $(1-\pi)$ of data points from a *complementing* distribution \bar{P}_j , representative of anomalies. Since we do not know what \bar{P}_j is, we will approximate it (heuristically) during training with a mixture over the other components in the training data. This results in the following corrupted version of P_j :

$$P_j^{\pi} := \pi P_j + (1 - \pi)\bar{P}_j, \qquad \bar{P}_j := \frac{1}{K - 1} \sum_{i \neq j} P_i$$
 (3)

We thereby choose π such that $\frac{1}{2} \ll \pi \le 1$. Analogously, we can define a test mixture distribution P_{\star}^{π} . This notation is fairly general and, in particular, captures the case where the training distribution is free of anomalies ($\pi = 1$). In Sec. 3.3, we will present a loss function that exploits artificial anomalies from \bar{P}_{j} during training.

Training Objective. We assume that optimizing our anomaly score $S_{\theta}(\mathbf{x}|P_j)$ can be achieved by minimizing a corresponding loss function $L_{\theta}(\mathbf{x}|P_j)$. Its parameters θ are shared across the different AD tasks j. In the simplest setup, this loss function is identical to the anomaly score,

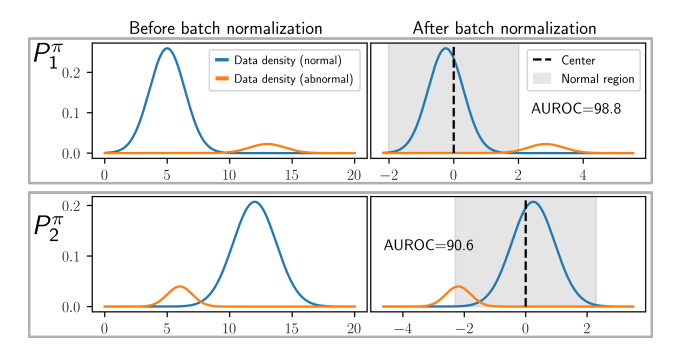


Figure 2. Illustration of batch normalization for AD with two tasks P_1^{π} and P_2^{π} . The method (batch-)normalizes the data in P_j^{π} separately. If each P_j^{π} consists mainly of normal samples, most samples will be shifted close to the origin (by subtracting the respective task's mean). As a result, the samples from all tasks concentrate around the origin in a joint feature space (gray area) and thus can be tightly enclosed using, e.g., one-class classification. Samples from the test task are batch normalized in the same way.

i.e., $L_{\theta}(\mathbf{x}|P_j) = S_{\theta}(\mathbf{x}|P_j)$, minimized over "normal" samples, but we also consider more sophisticated setups below. We thus study the following minimization problem:

$$\min_{\theta} \sum_{j=1}^{K} E_{\mathbf{x} \sim P_{j}^{\pi}} [L_{\theta}(\mathbf{x}|P_{j})]. \tag{4}$$

Typical choices for self-supervised training losses are DSVDD (Ruff et al., 2019) or neural transformation learning (NTL) (Qiu et al., 2021). Details will follow in Sec. 3.3.

Adapting to New Data Distributions. So far, we have left out how the anomaly score or loss function can depend on a training or test distribution P. We stress that our work assumes that, after training, we are not allowed to adjust any parameters θ to newly encountered distributions.

The key idea of our approach is to evaluate the anomaly scores not individually for single data points, but jointly based on a *mini-batch* $\mathbf{x}_{1:B} \stackrel{iid}{\sim} P$:

$$S_{\theta}(\mathbf{x}|P) \approx S_{\theta}(\mathbf{x}|\mathbf{x}_{1:B})$$

 $L_{\theta}(\mathbf{x}|P) \approx L_{\theta}(\mathbf{x}|\mathbf{x}_{1:B})$ (5)

Since distributions P typically encountered in AD practice dominantly consist of "normal" samples, information about P can be extracted from the mini-batch. The minimization problem then becomes

$$\min_{\theta} \sum_{j=1}^{K} E_{\left\{\mathbf{x}_{1:B}\right\}_{\sim}^{\text{i.i.d.}} P_{j}^{\pi}} \left[\sum_{i=1}^{B} L_{\theta}(\mathbf{x}_{i} | \mathbf{x}_{1:B}) \right]. \tag{6}$$

Next, we discuss another ingredient of the proposed method: batch normalization. We start with a motivating example.

Example. For illustration, let us first consider a simple outlier detector free of parameters θ :

$$S(\mathbf{x}|\mathbf{x}_{1:B}) = ||\mathbf{x} - \frac{1}{B} \sum_{j=1}^{B} \mathbf{x}_{j}||_{2}^{2}.$$
 (7)

If the \mathbf{x}_i lie in an informative feature space, anomalies will have a higher-than-usual distance to the mean, making the approach a simple, adaptive AD method.

While the example provides a proof of concept, in practice, the normal samples typically do not concentrate around their mean in the raw data space. Next, we develop an approach that learns to encode the samples (of potentially unseen test distributions) into a feature space where the intuition behind this example can be exploited for zero-shot AD.

Zero-shot Adaptation by Batch Normalization. The proposed method uses as anomaly score a neural network $S_{\theta}(\mathbf{x}|P) = f_{\theta}(\mathbf{x})$ with batch normalization layers and f_{θ} obtained by meta-training of Eq. (6).

The key idea—illustrated in Fig. 2—is to (batch-)normalize the normal data in each task (separately) so that each task is approximately centered around the origin (zero) and has variance one in neural feature space. In that way, the neural network adapts to the majority of data in a batch (the "new normal") to accomplish its training task.

The batch statistics $\{(\boldsymbol{\mu}_l, \boldsymbol{\sigma}_l)\}_{l=1}^L$ in all L layers are adaptive with $\{\mathbf{x}_i\}_{i=1}^B$. For every batch normalization layer with inputs $\{f_{\theta,l}(\mathbf{x}_i)\}_{i=1}^B$:

$$\mu_l = \sum_{i=1}^B f_{\theta,l}(\mathbf{x}_i)/B, \quad \boldsymbol{\sigma}_l = \left(\sum_{i=1}^B \left(f_{\theta,l}(\mathbf{x}_i) - \boldsymbol{\mu}_l\right)^2/B\right)^{1/2}.$$

All computations are point-wise. To preserve the adaptability of the batch normalization layers, all batch statistics $\{(\mu_l, \sigma_l)\}_{l=1}^L$ are computed on fly from the training/test samples. Since normal samples make up the majority of the batch, computing μ_l is dominated by normal samples.

As a result, regardless of the task, the distance to the origin defines a reasonable anomaly score. Remarkably, we obtain as a result an anomaly detector generalizing to unseen distributions without the need to adjust any model parameters.

3.3. Meta Outlier Exposure

We now discuss an important aspect of our approach that avoids trivial solutions in meta-learning. The approach builds on using labeled anomalies from \bar{P}_i during training.

As discussed in (Hendrycks et al., 2018; Qiu et al., 2022b), many anomaly scores $S_{\theta}(\mathbf{x}|P)$ allow for easily constructing a score $A_{\theta}(\mathbf{x}|P)$ that behaves inversely. That means, we expect $A_{\theta}(\mathbf{x}|P)$ to be *large* when evaluated on normal samples, and small for anomalies. Importantly, both scores

share the same parameters. In the context of DSVDD, we define $S_{\theta}(\mathbf{x}) = 1/A_{\theta}(\mathbf{x})$, but other definitions are possible for alternative losses (Ruff et al., 2018; 2019; Qiu et al., 2022b). Using the inverse score, we can construct a supervised AD loss on the meta training set as follows.

We define a task-sample indicator variable $y_{i,j}$ as

$$y_{i,j} = \begin{cases} 1 & \text{if } \mathbf{x}_i \in \bar{P}_j \\ 0 & \text{if } \mathbf{x}_i \in P_j \end{cases}, \tag{8}$$

which is also called an anomaly label. A natural choice for the loss in Eq. (6) is therefore

$$L_{\theta}(\mathbf{x}_{i}|\mathbf{x}_{1:B}) = (1 - y_{i,j})S_{\theta}(\mathbf{x}_{i}|\mathbf{x}_{1:B}) + y_{i,j}A_{\theta}(\mathbf{x}_{i}|\mathbf{x}_{1:B}).$$

The loss function resembles the outlier exposure loss of Hendrycks et al. (2018), but as opposed to using synthetically generated samples (typically only available for images), we use samples from the complement \bar{P}_j at training time to synthesize outliers.

In addition to DSVDD, we also study backbone models such as binary classifiers and NTL (Qiu et al., 2021). For NTL, we adopt the \mathbf{S}_{θ} and \mathbf{A}_{θ} used by Qiu et al. (2022b). For binary classifiers, we set $\mathbf{S}_{\theta}(\mathbf{x}) = -\log \left(1 - \sigma(f_{\theta}(\mathbf{x}))\right)$ and $\mathbf{A}_{\theta}(\mathbf{x}) = -\log \sigma(f_{\theta}(\mathbf{x}))$.

Meta Outlier Exposure avoids trivial solutions. The benefit of the outlier exposure loss in meta-training is that the learning algorithm cannot simply learn a model on the *average* data distribution, i.e., without learning to adapt. This failure to adapt is a common problem in meta-learning. Our solution relies on using each training sample \mathbf{x}_i in different contexts: depending on the sign of $y_{i,j}$, data point \mathbf{x}_i is considered normal (when drawn from P_j) or anomalous (when drawn from P_j). This ambiguity prevents the model from learning an average model over the meta data set and forces it to adapt to individual distributions instead.

4. Experiments

We evaluate the proposed method ACR on both image and tabular data when distribution shifts occur at test time. We compare ACR with established baselines from the deep AD, zero-shot AD, and few-shot AD. The experiments show that our method is suitable for different data types, applicable to diverse AD models, robust to various anomaly ratios, and significantly outperforms existing baselines.

We report results on image and tabular data in Sec. 4.1 and Sec. 4.2, and perform ablation studies in Sec. 4.3.

Practical Training and Testing. We construct training and test distributions using labeled datasets², where all x

from the same class j (e.g., all 0's in MNIST) are considered samples from the same P_j . The dataset \mathcal{Q} (e.g., MNIST as a whole) is the meta-set of all these distributions.

For training and testing, we split the meta-dataset into disjoint subsets. In the MNIST example, we define $P_0, ..., P_4$ as the distributions of images with digits 0-4 and use them for training. For testing, we select a single distribution of digits not seen during training (e.g., digit 5) as the "new normal" distribution P_* to which we adapt the model. The remaining digits (6-9) in this example) are used as test-time anomalies. To reduce variance, we rotate the roles among digits 5-9, using each digit as a test distribution once.³

4.1. Experiments on Images

We evaluate ACR on images when applied to two simple backbone models: DSVDD and a binary classifier. The evaluation demonstrates that our method achieves superior zero-shot AD results on natural images, hand-written characters, and medical images.

Image Datasets. We study four image datasets: CI-FAR100 (Krizhevsky et al., 2009)/CIFAR100-C (Hendrycks & Dietterich, 2019), Omniglot (Lake et al., 2015), MNIST (LeCun et al., 1998), and OrganA (Yang et al., 2021). CIFAR100 contains 100 classes of natural images, while the other datasets contain non-natural images. CIFAR100-C is the noise-corrupted version of CIFAR100's test data, thus considered as distributionally shifted data. We train using all training images from CIFAR100 and test all models on CIFAR100-C. Omniglot is a benchmark dataset for meta-learning. It has 1623 classes of hand-written characters, where each class comprises 20 images. All models are trained on the first 1200 classes and tested on the unseen 423 classes. MNIST has ten classes of hand-written digits. OrganA is a medical image dataset with 11 classes (for various body organs). On both MNIST and OrganA, we leave two successive classes out for testing and use the other classes for training. We repeat the evaluation on all combinations of two consecutive classes.

Image Baselines. We compare our proposed method with a state-of-the-art deep anomaly detector, a state-of-the-art zero-shot AD baseline, and a few-shot AD baseline.

Anomaly detection with an inductive bias (ADIB) (Deecke et al., 2021) is a state-of-the-art deep anomaly detector fine-tuning a pre-trained ResNet with outlier exposure (Hendrycks et al., 2018). It achieves an AUC of 99% on CIFAR-10, the highest reported number in the literature. CLIP-AD (Liznerski et al., 2022) is a zero-shot method based on the foundation model CLIP (Radford et al., 2021). CLIP-AD detects anomalies by comparing a test image

²these are either classification datasets (which have labels) or datasets where one of the covariates is binned to provide classes.

³This is the popular "one-vs-rest" testing set-up, which is standard in AD benchmarking. (e.g., (Ruff et al., 2021))

Table 1. AUC (%) with standard deviation for anomaly detection on CIFAR100-C with Gaussian noise or Gaussian Blur (Hendrycks & Dietterich, 2019). ACR with both backbone models perform best on images with Gaussian noise and outperform baselines except for CLIP-AD on images with Gaussian Blur.

		Gaussia	n Noise		Gaussian Blur			
	1%	5%	10%	20%	1%	5%	10%	20%
ADIB	50.9±2.4	50.5±0.9	50.6±0.9	50.2±0.5	50.1±1.4	51.1±1.4	49.9±1.0	49.8±0.3
Feat + BN	62.5 ± 3.1	61.8 ± 1.7	61.2 ± 0.6	60.2 ± 0.4	64.9 ± 1.5	65.3 ± 1.2	64.0 ± 0.9	62.7 ± 0.4
OC-MAML	53.0 ± 3.6	54.1 ± 1.9	55.8 ± 0.6	57.1 ± 1.0	55.6±3.6	56.6 ± 0.6	56.8 ± 1.1	57.6 ± 0.6
CLIP-AD	82.3 ± 1.1	82.6 ± 0.9	82.3 ± 0.9	82.6 ± 0.1	$91.9{\pm}0.8$	$92.7 \!\pm\! 0.5$	$92.1{\pm}0.5$	$92.3{\pm}0.2$
ACR-DSVDD	87.7±1.4	86.3±0.9	85.9±0.4	85.6±0.4	88.5±1.1	88.5±0.7	88.7±0.4	88.6±0.3
ACR-BCE	84.3 ± 2.2	$86.0{\pm}0.3$	$\pmb{86.0\!\pm\!0.2}$	$85.7 \!\pm\! 0.4$	85.6 ± 1.3	85.0 ± 0.6	85.0 ± 0.9	84.7 ± 0.5

Table 2. AUC (%) with standard deviation for anomaly detection on non-natural images: Omniglot, MNIST, and OrganA. ACR with both backbone models outperforms all baselines on all datasets. In comparison, CLIP-AD performs much worse on non-natural images.

	MNIST			OrganA			Omniglot		
	1%	5%	10%	1%	5%	10%	5%	10%	20%
ADIB	50.4±2.0	49.4±1.7	49.4±2.0	49.9±6.3	50.3±2.4	50.2±1.3	50.8±1.7	49.5±0.6	49.7±0.4
Feat + BN	80.0 ± 1.9	78.4 ± 1.5	74.9 ± 0.3	54.2 ± 1.7	53.5 ± 0.8	52.9 ± 0.3	88.1 ± 0.8	86.7 ± 0.5	84.4 ± 0.6
OC-MAML	83.7 ± 3.5	86.0 ± 2.3	86.4 ± 2.8	73.7 ± 4.7	72.2 ± 2.6	74.2 ± 2.4	98.6 ± 0.3	98.4 ± 0.2	98.5 ± 0.1
CLIP-AD	53.9 ± 1.4	53.7 ± 0.9	53.9 ± 0.8	52.6 ± 0.8	51.9 ± 0.6	51.5 ± 0.2	N/A	N/A	N/A
ACR-DSVDD ACR-BCE	91.9 ± 0.8 88.7±0.6	90.4 ± 0.2 87.8±0.4	88.8 ± 0.2 86.5±0.3	79.0±1.0 81.1 ± 0.8	77.7±0.4 79.5 ± 0.4	76.3±0.3 78.3 ± 0.3	99.1 ± 0.2 98.5±0.2	99.1±0.2 98.9±0.1	99.2±0.0 99.1±0.1

to a normal object's text description in a semantic space. Notice that running CLIP-AD requires a language description of the normal class, which can be a severe limitation in practice. One-class model-agnostic meta learning (OC-MAML) (Frikha et al., 2021) is a few-shot AD method trained with MAML (Finn et al., 2017). At test time, OC-MAML requires a few normal samples to update the model parameters. We implement OC-MAML using their officially released code with the same model architecture as our method. We always compare to 1-shot OC-MAML in our experiments. Feat+BN is a baseline for zero-shot AD on images, where we extract image features from a pre-trained ResNet and then apply batch normalization on the output to score anomalies based on the distance to the center. See Supp. A for more details.

Implementation Details. We use $\pi = 0.8$ in Eq. (3) to mix the training distributions from the different classes. For each approach, we train a single model and test it on different anomaly ratios. Two backbone models are implemented: DSVDD (ACR-DSVDD) and a binary classifier with cross entropy loss (ACR-BCE). More details are given in Supp. C.2.

Results. We report the results in terms of the AUROC averaged over five independent test runs with standard deviation. We apply the model to tasks with different anomaly ratios to study the robustness of ACR to the anomaly ratio at test time. The results on CIFAR100-C in Tab. 1⁴

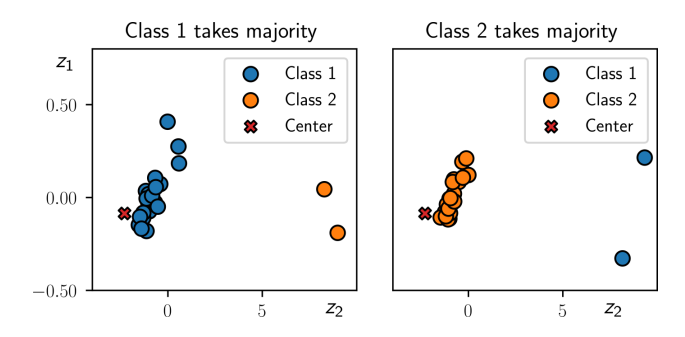


Figure 3. 2D visualization (after PCA) of the adaptively centered representations for two test tasks in the Omniglot dataset. The same learned DSVDD model adapts with our proposed method and maps samples from the majority class (class 1 (left) and class 2 (right)) to the same center in the embedding space in both tasks.

indicate that ACR outperforms ADIB, Feat+BN, and OC-MAML significantly. ACR achieves results competitive with CLIP-AD under various anomaly ratios. Although ADIB achieves good results when no distribution shift occurs (see results in Deecke et al. (2021)), ADIB is not able to generalize its performance to test data with distribution shifts. While the few-show method OC-MAML relies on a sufficiently large set of normal data for the adaptation, ACR requires no normal data at test time and achieves better results without any parameter updates. CLIP-AD has strong performance on CIFAR100C, presumably because it is trained on massive natural images from the internet (also covering CIFAR100/CIFAR100-C related images) rather than its adaptation ability. Also, CLIP-AD requires a text

⁴More results on CIFAR100-C are provided in Supp. C.

description of the normal class and therefore receives more annotation information at test time than ACR. Still, ACR outperforms CLIP-AD when the test images are corrupted with Gaussian noise.

We also evaluate the performance on non-natural images and report the results in Tab. 2. We can see that ACR consistently achieves the best results and significantly outperforms CLIP-AD. Since non-natural images are not included in the training set of CLIP, CLIP-AD does not perform well even on the simple MNIST dataset. Also, CLIP-AD cannot be applied on Omniglot since there is no available text description of the characters.

We provide a visualization of the learned representations from DSVDD on the Omniglot dataset as qualitative evidence in Fig. 3. We observe that even though the normal and abnormal data classes flip in two plots, the model learns to center the samples from the majority class and map the samples from the minority class away to the center in the embedding space. In conclusion, ACR is an easy-to-use zero-shot AD method and achieves superior zero-shot AD results on different types of images. The performance of ACR is also robust against the test anomaly ratios.

4.2. Experiments on Tabular Data

Tabular data is widely used in many real-world AD applications, e.g, network intrusion detection and malware detection. Distribution shifts in such data occur naturally over time (e.g., as new malware emerges), especially in a large time span. We evaluate ACR on tabular AD when applied to DSVDD and NTL. The evaluation shows that ACR achieves a new state-of-the-art of zero-shot AD on tabular data when distribution shifts occur.

Tabular Datasets. We evaluate all methods on two realworld tabular AD datasets: Anoshift (Dragoi et al., 2022) and Malware (Huynh et al., 2017).

Anoshift is a traffic dataset for network intrusion detection collected over ten years (2006-2015). We follow the preprocessing procedure and train/test split suggested in Dragoi et al. (2022). The model is trained on normal data collected from 2006 to 2010, validated on a mixture of normal and abnormal samples collected from 2006 to 2010, and tested on a mixture of normal and abnormal samples (with anomaly ratios varying from 1% to 20%) collected from 2011 to 2015. Dragoi et al. (2022) has observed that there are gradual distribution shifts in 2014 and 2015.

Malware is a dataset of malicious and benign computer programs, collected from 11/2010 to 07/2014. Malware attacks are designed adversarially, thus leading to shifts in both normal and abnormal data. We adopt the data reader from Li et al. (2021). We follow the preprocessing of (Huynh et al., 2017) and convert the real-valued probabilities p of being

malware to binary labels (labeled one if p > 0.6 and zero if p < 0.4). The samples with probabilities between 0.4 and 0.6 are discarded. The model is trained on normal samples collected from 01/2011 to 12/2013, validated on normal and abnormal samples from 11/2010 to 12/2010, and tested on normal and abnormal samples from 01/2014 to 07/2014 (the anomaly ratios vary between 1% and 20%).

Tabular Baselines. We compare with state-of-the art deep and shallow detectors for tabular AD (Dragoi et al., 2022; Alvarez et al., 2022; Han et al., 2022) and study their performance under test distribution shifts. The shallow AD baselines include OC-SVM (Schölkopf et al., 1999), IForest (Liu et al., 2012), LOF (Breunig et al., 2000), and KNN (Ramaswamy et al., 2000). The deep AD baselines include DSVDD (Ruff et al., 2018), Autoencoder (AE) (Aggarwal, 2017), LUNAR (Goodge et al., 2022), internal contrastive learning (ICL) (Shenkar & Wolf, 2021), NTL (Qiu et al., 2021), and BERT (Kenton & Toutanova, 2019; Dragoi et al., 2022). We adopt the implementations from PyOD (Han et al., 2022) or their official repositories.

Implementation Details. Since Anoshift and Malware do not have labels we use the collection date as class labels for separating the data into training distributions P_j (year for Anoshift and month for Malware). The training tasks are mixed with anomaly ratio $\pi = 0.8$. To create more training tasks, we augment the data using attribute permutations, resulting in additional training distributions. These attribute permutations increase the variability of training tasks and encourage the model to learn permutation-invariant features. In testing tasks, the attributes are not permuted.

ACR-NTL has the same model architecture as the baseline NTL, and ACR-DSVDD adds one additional batch normalization layer on top of the DSVDD baseline. Details of the model architectures are provided in Supp. B. Our algorithm is applicable to the existing backbone models without complex modifications.

Results. In Tab. 3, we report the results on Anoshift split into AVG (data from 2011 to 2015) and FAR (data from 2014 and 2015). The two splits allow us to compare average detection accuracy (AVG) with detection results after longer time intervals (FAR) which is expected to suffer from more distribution shift. For evaluating ACR's robustness to variations in the anomaly ratio, we report results on test data with a ratio varying from 1% to 20%. We report average AUC with standard deviation over five independent test runs.

The results in Tab. 3, show that ACR outperforms all baselines on both FAR and AVG under all anomaly ratios. ACR is the only method that clearly outperforms random guessing on the FAR split. All baselines perform worse than random on the FAR split even though they achieve strong results when there is no distribution shifts (see results in Dragoi

Table 3. AUC (%) with standard deviation for anomaly detection on Anoshift (Dragoi et al., 2022). ACR with both backbone models outperforms all baselines on average over time spans other than the training set. Especially, ACR is the single method performs clearly better than random guess on FAR split where distribution shift occurs.

	1	%	5	%	10	1%	20)%
	FAR	AVG	FAR	AVG	FAR	AVG	FAR	AVG
OC-SVM	49.6±0.2	62.6±0.1	49.6±0.2	62.6±0.1	49.5±0.1	62.7±0.1	49.5±0.1	62.6±0.1
IForest	25.8 ± 0.4	54.6 ± 0.2	26.1 ± 0.1	54.7 ± 0.1	26.0 ± 0.1	54.6 ± 0.1	26.0 ± 0.1	54.7 ± 0.1
LOF	37.3 ± 0.5	59.6 ± 0.3	37.0 ± 0.1	59.5 ± 0.1	37.0 ± 0.1	59.5 ± 0.1	37.1 ± 0.1	59.5 ± 0.1
KNN	45.0 ± 0.3	70.8 ± 0.1	45.3 ± 0.2	70.9 ± 0.1	45.1 ± 0.1	70.8 ± 0.1	45.2 ± 0.1	70.8 ± 0.1
DSVDD	34.6±0.3	62.3±0.2	34.7±0.1	62.5±0.1	34.7±0.2	62.5±0.1	34.7±0.1	62.5±0.1
AE	18.6 ± 0.2	25.3 ± 0.1	18.7 ± 0.2	25.5 ± 0.1	18.7 ± 0.1	25.5 ± 0.1	18.7 ± 0.1	25.5 ± 0.1
LUNAR	24.5 ± 0.4	38.3 ± 0.4	24.6 ± 0.1	38.6 ± 0.2	24.7 ± 0.1	38.7 ± 0.1	24.6 ± 0.1	38.6 ± 0.1
ICL	20.6 ± 0.3	50.5 ± 0.2	20.7 ± 0.2	50.4 ± 0.1	20.7 ± 0.1	50.4 ± 0.1	20.8 ± 0.1	50.4 ± 0.1
NTL	40.7 ± 0.3	57.0 ± 0.1	40.9 ± 0.2	57.1 ± 0.1	41.0 ± 0.1	57.1 ± 0.1	41.0 ± 0.1	57.1 ± 0.1
BERT	28.6 ± 0.3	64.6 ± 0.2	28.7 ± 0.1	64.6 ± 0.1	28.7 ± 0.1	64.6 ± 0.1	28.7 ± 0.1	64.7 ± 0.1
ACR-DSVDD ACR-NTL	62.0±0.5 62.5±0.2	74.0 ± 0.2 73.4±0.1	61.3±0.1 62.2±0.1	73.3±0.1 73.2±0.1	60.4±0.1 62.3±0.1	72.5±0.1 73.1±0.1	59.1±0.1 62.0 ± 0.1	71.2±0.1 72.7 ± 0.1
ACK-NIL	02.5±0.2	/3.4±0.1	04.4±0.1	/3.4±0.1	02.3±0.1	/3.1±0.1	02.0±0.1	/ 4. / ±0.1

Table 4. AUC (%) with standard deviation for anomaly detection on Malware (Huynh et al., 2017). ACR-NTL achieves the best results on various anomaly ratios.

	1%	5%	10%	20%
OC-SVM	19.5±5.6	20.5±1.4	20.3±0.9	20.3±0.8
IForest	22.8 ± 2.9	22.9 ± 1.2	23.3 ± 0.6	23.4 ± 0.8
LOF	22.3 ± 4.9	23.2 ± 1.8	23.3 ± 1.3	23.2 ± 0.4
KNN	21.6 ± 6.3	22.5 ± 1.6	22.7 ± 0.9	22.6 ± 0.9
DSVDD	25.4±3.3	27.4±1.7	28.9±0.9	28.3±0.8
AE	48.8 ± 2.4	49.1 ± 1.2	49.4 ± 0.6	49.3 ± 0.5
LUNAR	23.1 ± 4.5	23.8 ± 1.2	24.1 ± 0.7	24.2 ± 0.6
ICL	83.5 ± 1.9	81.0 ± 1.0	82.9 ± 0.8	83.1 ± 0.9
NTL	25.9 ± 4.8	25.4 ± 1.3	24.5 ± 1.3	25.0 ± 0.8
ACR-DSVDD ACR-NTL	73.1±2.8 85.0 ± 1.3	69.5±3.3 84.5 ± 0.8	69.4±3.3 85.1 ± 1.2	66.4±4.0 84.0 ± 0.8

et al. (2022); Alvarez et al. (2022); Han et al. (2022)).

Although we can see that ACR achieves the best results on all anomaly ratios, the performance of ACR degrades when the ratio increases. ACR-NTL is more robust to high anomaly ratios than ACR-DSVDD. As the anomaly ratio increases, it becomes harder to identify the majority among the mixture of normal samples and anomalies.

We report the results on Malware in Tab. 4. ACR-NTL achieves the best results under all anomaly ratios. All baselines except ICL perform worse than random guessing, meaning that the malware successfully fools most baselines.

4.3. Ablation Study

We perform two ablation studies, one to demonstrate the benefit of our proposed meta outlier exposure loss, and one to study the behavior of batch normalization during training.

To show that meta outlier exposure is a favorable option, we compare it against the one-class classification loss and a fine-tuned version of Feat+BN, where the pretrained ImageNet features are finetuned on domain-specific training data. Tab. 5 shows that our approach outperforms the two alternatives on two image datasets. To analyze batch normalization variants, we train and test models with different combinations of batch normalization usage detailed inTab. 6. We find that for effective zero-shot AD, the batch normalization statistics should be computed on the fly both during testing and training. More details are in Supp. C.1.

5. Conclusion

We studied the problem of adapting a learned AD method to a new data distribution, where the concept of "normality" changed. Our method is a zero-shot approach and requires no training or fine-tuning to a new data set. We developed a new meta-training approach, where we trained an off-the-shelf deep AD method on a (meta-) set of interrelated datasets, adopting batch normalization in every layer, and used samples from the meta set as either normal samples and anomalies, depending on the context. We showed that the approach robustly generalized to new, unseen anomalies.

Our experiments on image and tabular data demonstrated state-of-the-art zero-shot adaptation performance when no foundation model was available. We stress that this is an important result since many, if not most AD applications in the real world rely on specialized datasets: medical images, data from industrial assembly lines, malware data, network intrusion data etc. Existing foundation models often do not capture these data, as we showed. Ultimately, our analysis shows that with relatively small modifications to model training (meta-learning, batch normalization, and providing artificial anomalies from the meta-set) will enable the deployment of existing models in zero-shot learning tasks.

Limitations & Societal Impacts Our method is primarily limited by the assumption that a meta-dataset is available that is related to the new dataset of interest. If this assumption is broken, zero-shot adaptation cannot be assured.

Anomaly detectors are trained to detect atypical/underrepresented data in a data set. Therefore, deploying an anomaly detector, e.g., in video surveillance, may ultimately discriminate against under-represented groups. Anomaly detection methods should therefore be critically reviewed when deployed on human data.

Acknowledgements

SM acknowledges support by the National Science Foundation (NSF) under an NSF CAREER Award, award numbers 2003237 and 2007719, by the Department of Energy under grant DE-SC0022331, by the HPI Research Center in Machine Learning and Data Science at UC Irvine, and by gifts from Qualcomm and Disney. Part of this work was conducted within the DFG research unit FOR 5359 on Deep Learning on Sparse Chemical Process Data. MK acknowledges support by the Carl-Zeiss Foundation, the DFG awards KL 2698/2-1, KL 2698/5-1, KL 2698/6-1, and KL 2698/7-1, and the BMBF awards 03—B0770E and 01—S21010C. We thank Eliot Wong-Toi for helpful feedback on the manuscript.

The Bosch Group is carbon neutral. Administration, manufacturing and research activities do no longer leave a carbon footprint. This also includes GPU clusters on which the experiments have been performed.

References

- Aggarwal, C. C. An introduction to outlier analysis. In *Outlier analysis*, pp. 1–34. Springer, 2017.
- Alvarez, M., Verdier, J.-C., Nkashama, D. K., Frappier, M., Tardif, P.-M., and Kabanza, F. A revealing large-scale evaluation of unsupervised anomaly detection algorithms. *arXiv* preprint arXiv:2204.09825, 2022.
- Baxter, J. A model of inductive bias learning. *Journal of artificial intelligence research*, 12:149–198, 2000.
- Bergman, L. and Hoshen, Y. Classification-based anomaly detection for general data. In *International Conference on Learning Representations*, 2020.
- Breunig, M. M., Kriegel, H.-P., Ng, R. T., and Sander, J. Lof: identifying density-based local outliers. In *Proceedings* of the 2000 ACM SIGMOD international conference on Management of data, pp. 93–104, 2000.
- Brown, T., Mann, B., Ryder, N., Subbiah, M., Kaplan, J. D., Dhariwal, P., Neelakantan, A., Shyam, P., Sastry, G.,

- Askell, A., et al. Language models are few-shot learners. *Advances in neural information processing systems*, 33: 1877–1901, 2020.
- Chen, B., Bondi, L., and Das, S. Learning to adapt to domain shifts with few-shot samples in anomalous sound detection. In 2022 26th International Conference on Pattern Recognition (ICPR), pp. 133–139. IEEE, 2022.
- Chen, X. and Konukoglu, E. Unsupervised detection of lesions in brain mri using constrained adversarial autoencoders. In *MIDL Conference book*. MIDL, 2018.
- Cohen, G., Afshar, S., Tapson, J., and Van Schaik, A. Emnist: Extending mnist to handwritten letters. In *2017 international joint conference on neural networks (IJCNN)*, pp. 2921–2926. IEEE, 2017.
- Deecke, L., Vandermeulen, R., Ruff, L., Mandt, S., and Kloft, M. Image anomaly detection with generative adversarial networks. In *Joint european conference on machine learning and knowledge discovery in databases*, pp. 3–17. Springer, 2018.
- Deecke, L., Ruff, L., Vandermeulen, R. A., and Bilen, H. Transfer-based semantic anomaly detection. In *International Conference on Machine Learning*, pp. 2546–2558. PMLR, 2021.
- Ding, K., Zhou, Q., Tong, H., and Liu, H. Few-shot network anomaly detection via cross-network meta-learning. *Proceedings of the Web Conference* 2021, 2021.
- Dragoi, M., Burceanu, E., Haller, E., Manolache, A., and Brad, F. Anoshift: A distribution shift benchmark for unsupervised anomaly detection. In *Thirty-sixth Conference on Neural Information Processing Systems Datasets and Benchmarks Track*, 2022.
- Esmaeilpour, S., Liu, B., Robertson, E., and Shu, L. Zeroshot out-of-distribution detection based on the pretrained model clip. In *Proceedings of the AAAI conference on artificial intelligence*, 2022.
- Feng, T., Qi, Q., Wang, J., and Liao, J. Few-shot class-adaptive anomaly detection with model-agnostic meta-learning. 2021 IFIP Networking Conference (IFIP Networking), pp. 1–9, 2021.
- Finn, C., Abbeel, P., and Levine, S. Model-agnostic metalearning for fast adaptation of deep networks. In *Interna*tional conference on machine learning, pp. 1126–1135. PMLR, 2017.
- Frikha, A., Krompaß, D., Köpken, H.-G., and Tresp, V. Fewshot one-class classification via meta-learning. *Proceed*ings of the AAAI Conference on Artificial Intelligence, 35 (8):7448–7456, May 2021.

- Golan, I. and El-Yaniv, R. Deep anomaly detection using geometric transformations. In *Advances in Neural Information Processing Systems*, pp. 9758–9769, 2018.
- Goodge, A., Hooi, B., Ng, S.-K., and Ng, W. S. Lunar: Unifying local outlier detection methods via graph neural networks. In *Proceedings of the AAAI Conference on Artificial Intelligence*, volume 36, pp. 6737–6745, 2022.
- Han, S., Hu, X., Huang, H., Jiang, M., and Zhao, Y. Adbench: Anomaly detection benchmark. In *Thirty-sixth Conference on Neural Information Processing Systems Datasets and Benchmarks Track*, 2022.
- He, K., Chen, X., Xie, S., Li, Y., Dollár, P., and Girshick, R. Masked autoencoders are scalable vision learners. In Proceedings of the IEEE/CVF Conference on Computer Vision and Pattern Recognition, pp. 16000–16009, 2022.
- Hendrycks, D. and Dietterich, T. Benchmarking neural network robustness to common corruptions and perturbations. In *International Conference on Learning Represen*tations, 2019.
- Hendrycks, D., Mazeika, M., and Dietterich, T. Deep anomaly detection with outlier exposure. In *International Conference on Learning Representations*, 2018.
- Hendrycks, D., Mazeika, M., Kadavath, S., and Song, D. Using self-supervised learning can improve model robustness and uncertainty. *Advances in Neural Information Processing Systems*, 32:15663–15674, 2019.
- Huynh, N. A., Ng, W. K., and Ariyapala, K. A new adaptive learning algorithm and its application to online malware detection. In *International Conference on Discovery Science*, pp. 18–32. Springer, 2017.
- Jia, C., Yang, Y., Xia, Y., Chen, Y.-T., Parekh, Z., Pham, H., Le, Q., Sung, Y.-H., Li, Z., and Duerig, T. Scaling up visual and vision-language representation learning with noisy text supervision. In *International Conference on Machine Learning*, pp. 4904–4916. PMLR, 2021.
- Kenton, J. D. M.-W. C. and Toutanova, L. K. Bert: Pretraining of deep bidirectional transformers for language understanding. In *Proceedings of naacL-HLT*, pp. 4171– 4186, 2019.
- Kozerawski, J. and Turk, M. A. Clear: Cumulative learning for one-shot one-class image recognition. 2018 IEEE/CVF Conference on Computer Vision and Pattern Recognition, pp. 3446–3455, 2018.
- Krizhevsky, A., Hinton, G., et al. Learning multiple layers of features from tiny images. 2009.
- Kruspe, A. One-way prototypical networks. *ArXiv*, abs/1906.00820, 2019.

- Lake, B. M., Salakhutdinov, R., and Tenenbaum, J. B. Human-level concept learning through probabilistic program induction. *Science*, 350(6266):1332–1338, 2015.
- LeCun, Y., Bottou, L., Bengio, Y., and Haffner, P. Gradient-based learning applied to document recognition. *Proceedings of the IEEE*, 86(11):2278–2324, 1998.
- Li, A., Boyd, A., Smyth, P., and Mandt, S. Detecting and adapting to irregular distribution shifts in bayesian online learning. *Advances in neural information processing systems*, 34:6816–6828, 2021.
- Liu, F. T., Ting, K. M., and Zhou, Z.-H. Isolation-based anomaly detection. *ACM Transactions on Knowledge Discovery from Data (TKDD)*, 6(1):1–39, 2012.
- Liznerski, P., Ruff, L., Vandermeulen, R. A., Franks, B. J., Muller, K. R., and Kloft, M. Exposing outlier exposure: What can be learned from few, one, and zero outlier images. *Transactions on Machine Learning Research*, 2022.
- Lu, Y., Yu, F., Reddy, M. K. K., and Wang, Y. Few-shot scene-adaptive anomaly detection. In *ECCV*, 2020.
- Principi, E., Vesperini, F., Squartini, S., and Piazza, F. Acoustic novelty detection with adversarial autoencoders. In 2017 International Joint Conference on Neural Networks (IJCNN), pp. 3324–3330. IEEE, 2017.
- Qiu, C., Pfrommer, T., Kloft, M., Mandt, S., and Rudolph, M. Neural transformation learning for deep anomaly detection beyond images. In *International Conference on Machine Learning*, pp. 8703–8714. PMLR, 2021.
- Qiu, C., Kloft, M., Mandt, S., and Rudolph, M. Raising the bar in graph-level anomaly detection. In *Proceed*ings of the Thirty-First International Joint Conference on Artificial Intelligence, IJCAI-22, pp. 2196–2203, 2022a.
- Qiu, C., Li, A., Kloft, M., Rudolph, M., and Mandt, S. Latent outlier exposure for anomaly detection with contaminated data. In Chaudhuri, K., Jegelka, S., Song, L., Szepesvari, C., Niu, G., and Sabato, S. (eds.), Proceedings of the 39th International Conference on Machine Learning, volume 162 of Proceedings of Machine Learning Research, pp. 18153–18167. PMLR, 17–23 Jul 2022b. URL https://proceedings.mlr.press/v162/qiu22b.html.
- Radford, A., Kim, J. W., Hallacy, C., Ramesh, A., Goh, G., Agarwal, S., Sastry, G., Askell, A., Mishkin, P., Clark, J., et al. Learning transferable visual models from natural language supervision. In *International Conference on Machine Learning*, pp. 8748–8763. PMLR, 2021.

- Ramaswamy, S., Rastogi, R., and Shim, K. Efficient algorithms for mining outliers from large data sets. In *Proceedings of the 2000 ACM SIGMOD international conference on Management of data*, pp. 427–438, 2000.
- Ruff, L., Vandermeulen, R., Goernitz, N., Deecke, L., Siddiqui, S. A., Binder, A., Müller, E., and Kloft, M. Deep one-class classification. In *International conference on machine learning*, pp. 4393–4402. PMLR, 2018.
- Ruff, L., Vandermeulen, R. A., Görnitz, N., Binder, A., Müller, E., Müller, K.-R., and Kloft, M. Deep semisupervised anomaly detection. In *International Conference on Learning Representations*, 2019.
- Ruff, L., Kauffmann, J. R., Vandermeulen, R. A., Montavon, G., Samek, W., Kloft, M., Dietterich, T. G., and Müller, K.-R. A unifying review of deep and shallow anomaly detection. *Proceedings of the IEEE*, 2021.
- Schlegl, T., Seeböck, P., Waldstein, S. M., Schmidt-Erfurth, U., and Langs, G. Unsupervised anomaly detection with generative adversarial networks to guide marker discovery. In *International conference on information process*ing in medical imaging, pp. 146–157. Springer, 2017.
- Schneider, T., Qiu, C., Kloft, M., Latif, D. A., Staab, S., Mandt, S., and Rudolph, M. Detecting anomalies within time series using local neural transformations. *arXiv* preprint arXiv:2202.03944, 2022.
- Schölkopf, B., Williamson, R. C., Smola, A., Shawe-Taylor, J., and Platt, J. Support vector method for novelty detection. *Advances in neural information processing systems*, 12, 1999.
- Schölkopf, B., Platt, J. C., Shawe-Taylor, J., Smola, A. J., and Williamson, R. C. Estimating the support of a highdimensional distribution. *Neural computation*, 13(7): 1443–1471, 2001.
- Schwartz, E., Arbelle, A., Karlinsky, L., Harary, S., Scheidegger, F., Doveh, S., and Giryes, R. Maeday: Mae for few and zero shot anomaly-detection. arXiv preprint arXiv:2211.14307, 2022.
- Shenkar, T. and Wolf, L. Anomaly detection for tabular data with internal contrastive learning. In *International Conference on Learning Representations*, 2021.
- Sheynin, S., Benaim, S., and Wolf, L. A hierarchical transformation-discriminating generative model for few shot anomaly detection. In *Proceedings of the IEEE/CVF International Conference on Computer Vision (ICCV)*, pp. 8495–8504, October 2021.

- Sohn, K., Li, C.-L., Yoon, J., Jin, M., and Pfister, T. Learning and evaluating representations for deep one-class classification. In *International Conference on Learning Representations*, 2020.
- Wang, Z., Zhou, Y., Wang, R., Lin, T.-Y., Shah, A., and Lim, S.-N. Few-shot fast-adaptive anomaly detection. In *Advances in Neural Information Processing Systems*, 2022.
- Wu, J.-C., Chen, D.-J., Fuh, C.-S., and Liu, T.-L. Learning unsupervised metaformer for anomaly detection. In *Proceedings of the IEEE/CVF International Conference on Computer Vision (ICCV)*, pp. 4369–4378, October 2021.
- Yang, J., Shi, R., and Ni, B. Medmnist classification decathlon: A lightweight automl benchmark for medical image analysis. In 2021 IEEE 18th International Symposium on Biomedical Imaging (ISBI), pp. 191–195. IEEE, 2021.
- Yu, J., Wang, Z., Vasudevan, V., Yeung, L., Seyedhosseini, M., and Wu, Y. Coca: Contrastive captioners are imagetext foundation models. *Transactions on Machine Learn*ing Research, 2022.
- Yuan, L., Chen, D., Chen, Y.-L., Codella, N., Dai, X., Gao, J., Hu, H., Huang, X., Li, B., Li, C., et al. Florence: A new foundation model for computer vision. *arXiv preprint arXiv:2111.11432*, 2021.
- Zhang, S., Ye, F., Wang, B., and Habetler, T. G. Few-shot bearing anomaly detection via model-agnostic meta-learning. 2020 23rd International Conference on Electrical Machines and Systems (ICEMS), pp. 1341–1346, 2020.
- Zhou, C. and Paffenroth, R. C. Anomaly detection with robust deep autoencoders. In *Proceedings of the 23rd ACM SIGKDD international conference on knowledge discovery and data mining*, pp. 665–674, 2017.

A. Baselines

CLIP-AD (**Liznerski et al., 2022**). CLIP (Contrastive Language–Image Pre-training (Radford et al., 2021)) is a pre-trained visual representation learning model that builds on open-source images and their natural language supervision signal. The resulting network projects visual images and language descriptions into the same feature space. The pre-trained model can provide meaningful representations for downstream tasks such as image classification and anomaly detection. When applying CLIP on zero-shot anomaly detection, CLIP prepares a pair of natural language descriptions for normal and abnormal data: $\{l_n = \text{``A photo of } \{\text{NORMAL_CLASS}\}$ ", $l_a = \text{``A photo of } \text{something}$ "}. The anomaly score of a test image x is the relative distance between x to l_n and x to l_a in the feature space,

$$s(\boldsymbol{x}) = \frac{\exp(\langle f_x(\boldsymbol{x}), f_l(l_a) \rangle)}{\sum_{c \in \{l_n, l_a\}} \exp(\langle f_x(\boldsymbol{x}), f_l(c) \rangle)},$$

where f_x and f_l are the CLIP image and description feature extractors and $\langle \cdot, \cdot \rangle$ is the inner product. We name this baseline CLIP-AD.

Compared to our proposed method, CLIP-AD requires a meaningful language description for the image. However, this is not always feasible for all image datasets like Omniglot (Lake et al., 2015), where people can't name the written characters easily. In addition, CLIP-AD doesn't apply to other data types like tabular data or time-series data. Finally, CLIP-AD has limited ability to adapt to a different data distribution other than its training one. These limitations are demonstrated in our experiments.

OC-MAML (Frikha et al., 2021). One-Class Model Agnostic Meta Learning (OC-MAML) is a meta-learning algorithm that taylors MAML (Finn et al., 2017) toward few-shot anomaly detection setup. OC-MAML learns a global model parameterization θ that can quickly adapt to unseen tasks with a few new task data points S, called a support set. The new-task adaptation takes the global model parameters to a task-specific parameterization $\phi(\theta, S_t)$ that has a low loss $L(Q_t; \phi(\theta, S_t))$ on the new task t, represented by another dataset Q_t , called a query set. OC-MAML uses a one-class support set to update the model parameters θ with a few gradient steps to get ϕ . To learn an easy-to-adapt global parameterization θ , OC-MAML directly minimizes the target loss on lots of training tasks. Suppose there are T tasks for training. The following loss function is minimized

$$l(\theta) = \frac{1}{T} \sum_{t=1}^{T} \mathbb{E}_{S_t \sim p_S^t, Q_t \sim p_Q^t} [L(Q_t; \phi(\theta, S_t))], \tag{9}$$

where p_S^t is task t's support set distribution and p_Q^t is the query set distribution. During training, the support set contains K normal data points where K is usually small, termed K-shot OC-MAML. The query set contains an equal number of normal and abnormal data and provides optimization gradients for θ . During test time, OC-MAML adapts the global parameter θ on the unseen task's support set S^* , resulting in a task-specific parameter $\phi(\theta, S^*)$. The newly adapted parameters are then used for downstream tasks.

OC-MAML is not a zero-shot anomaly detector and requires K support data points to adapt compared to our method. Our method is simpler in training as it doesn't need to adapt to the support set with additional gradient updates, characterized in the function $\phi(\theta, S)$. OC-MAML is also different in batch normalization. Rather than the original batch normalization, OC-MAML first computes the batch moments using the support set and then normalizes both the support and query set with the same moments. However, the computed moments can be noisy when the support set size is small. In our experiments, we adopt a 1-shot OC-MAML for all image data.

Pre-trained features + BN. Because batch normalization is an effective tool for zero-shot anomaly detection (see Fig. 2), we directly apply batch normalization on extracted features from a pre-trained model. We then compute the anomaly score as the Euclidean distance between a feature vector and the origin in the feature space. Our experiments use a ResNet152 model pre-trained on ImageNet as a feature extractor and extract its 2048-dimension penultimate layer output as the final feature vector. We name this baseline Pre-trained features + BN. Pre-trained features + BN doesn't optimize the feature extractor jointly with the zero-shot detection property of batch normalization. Hence the extracted pre-trained features are not optimal for the zero-shot anomaly detector – batch normalization.

ADIB (Deecke et al., 2021). In addition to zero-shot and few-shot anomaly detectors, we also compare with the state-of-the-art deep anomaly detector ADIB (Deecke et al., 2021) which use pre-trained image features and additional data for

outlier exposure in training. We use a "debiased" subset of TinyImageNet as the outlier exposure data for CIFAR100 as suggested in Hendrycks et al. (2018), use EMNIST (Cohen et al., 2017) as the outlier exposure data for MNIST as suggested in Liznerski et al. (2022), use OrganC and OrganS datasets (Yang et al., 2021) as outlier exposure data for OrganA, and use half of the training data as normal data and half of the training data as auxiliary outliers for Omniglot.

B. Implementation Details

B.1. Implementation Details on Image Data

Training protocols. We train the model 6,000 iterations on CIFAR100 data, 10,000 iterations on Omiglot, and 2,000 iterations on MNIST and OrganA. Each iteration contains 32 training tasks; each task mini-batch has 30 (for datasets other than CIFAR100) or 60 (for CIFAR100) points sampled from $P_j^{0.8}$. All 32 training tasks' gradients are averaged and incur one gradient update per iteration.

ACR-DSVDD. We use the standard convolutional neural network architecture used in meta-learning. Specifically, the network contains four convolution layers. Each convolution layer is followed by a batch normalization layer and a ReLU activation layer. The final layer is a fully-connectly layer followed by a batch normalization layer. The center of DSVDD has the same dimension as the output of the fully-connected layer, which is 32. For CIFAR100/CIFAR100-C, each convolution layer has 128 kernels. For MNIST, Omniglot, and OrganA, each convolution layer has 64 kernels. Each kernel's size is 3x3. We use Adam with a learning rate of 0.003 on CIFAR100 dataset and 1e-4 on all the other datasets.

ACR-BCE. We use the same network structure as ACR-DSVDD without the final batch normalization layer and the center. The final fully-connected layer has output dimension of 1. We train the model with binary cross entropy loss. We use Adam with a learning rate of 0.003 on CIFAR100 dataset and 1e-4 on all the other datasets.

B.2. Implementation Details on Tabular Data

ACR-DSVDD. ACR is applied to the backbone model DSVDD (Ruff et al., 2018). The neural network of DSVDD is a four-layer MLP with intermediate batch normalization layers and ReLU activations. The hidden sizes on Anoshift dataset are [128, 128, 128, 128, 32]. The hidden sizes on Malware dataset are [64, 64, 64, 32]. One batch normalization layer is added on the top of the network on Anoshift experiment. The statistics of all batch normalization layers are computed on fly on the training/test batches. We use Adam with a learning rate of 4e-4 on Anoshift dataset and 1e-4 on Malware dataset.

ACR-NTL. ACR is applied to the backbone model NTL (Qiu et al., 2021). The shared encoder of NTL is a four-layer MLP with intermediate batch normalization layers and ReLU activations. The hidden sizes of the encoder are [128, 128, 128, 32]. The statistics of all batch normalization layers are computed on fly on the training/test batches. We set the number of neural transformations as 19. Each neural transformation is parametrized by a three-layer MLP of hidden size of 128 with ReLU activations. All networks are optimized jointly with Adam with a learning rate of 4e-4.

C. Additional Results

C.1. Ablation Study

Training with different losses. We study the benefits of using meta outlier exposure in Eq. (6) and compare to a) using one-class classification loss $L_{\theta}(\mathbf{x}|\mathbf{x}_{1:B}) = S_{\theta}(\mathbf{x}|\mathbf{x}_{1:B})$ with $S_{\theta}(\mathbf{x}) = ||f_{\theta}(\mathbf{x}) - \mathbf{c}||^2$, b) (data-adapted) Feat+BN. The data-adapted Feat+BN first learns the features by performing a multi-class classification task with the training set. Then a batch normalization layer is applied on the top of penultimate layer representations for zero-shot anomaly detection. We train a 100-class classifier for CIFAR100C and Omniglot separately. Note that for Omniglot, we randomly sub-sample 100 classes from its 1400 training classes and train the classifier. From the results in Tab. 5 we can see that both ablations perform competitive with ACR on the simple Omniglot dataset, but perform much worse compared to ACR on the complex CIFAR100-C dataset. In conclusion, using meta outlier exposure in training is favorable.

Training Without BatchNorm. We investigate whether training without batch normalization works for zero-shot AD or not. To this end, we employ four different combinations of batch normalization usage during training and testing and check which combination works and which doesn't. We trained the models with the same meta-training procedure as what we used

Table 5. AUC (%) with standard deviation for anomaly detection on CIFAR100-C and Omniglot. As an ablation, rather than utilizing outlier exposure, we trained Zero-shot BN only on normal data of each task.

	CIFAR100-C (Gaussian Noise)				Omniglot		
	1%	5%	10%	20%	5%	10%	20%
OCloss	72.2±2.2	73.9±1.4	74.2±0.9	73.8±0.3	96.2±1.0	96.4±0.8	96.2±0.8
(data-adapted) Feat+BN	70.9 ± 2.2	67.6 ± 0.2	67.0 ± 0.7	64.9 ± 0.5	99.2 ± 0.2	99.1±0.1	99.0 ± 0.1

Table 6. The effects of batch normalization for zero-shot AD. The first two columns show different combinations of batch normalization usage during training and testing. The third column answers the question whether the type of batchnorm usage works for zero-shot AD.

BatchNorm (train)	BatchNorm (test)	Work?
✓	✓	Yes
✓	X	No
X	✓	No
	×	No

in Sec. 4.1 and tested on CIFAR100-C and Omniglot and present the results in Tab. 6. In the third column, "Yes" indicates the AUROC metric is significantly larger than 0.5, and therefore learns a meaningful zero-shot AD model; "No" indicates the AUROC performance is around 0.5, which means the predicted anomaly scores are like random guess and the model cannot be used for zero-shot AD. Tab. 6 shows that only when the batch normalization is used both in training and testing, the zero-shot AD works. Otherwise, the meta-training procedure couldn't result in meaningful zero-shot AD representations.

Moreover, for the Deep SVDD model, we can theoretically show that training without batch normalization won't work with meta outlier exposure: the optimal loss function has nothing to do with zero-shot AD. Rather, the optimal loss is only related to the mixture weight π during training. Without loss of generality, suppose we have two training distributions P_1, P_2 . We learn a Deep SVDD model parameterized by θ and c by the meta outlier exposure method,

$$l(\theta,c) = \mathbb{E}_{x \sim P_1^{\pi}} \left[(1 - y_1)(f_{\theta}(x) - c)^2 + \frac{y_1}{(f_{\theta}(x) - c)^2} \right] + \mathbb{E}_{x \sim P_2^{\pi}} \left[(1 - y_2)(f_{\theta}(x) - c)^2 + \frac{y_2}{(f_{\theta}(x) - c)^2} \right]$$
(10)

$$= \mathbb{E}_{x_1 \sim P_1, x_2 \sim P_2} \left[\pi (f_{\theta}(x_1) - c)^2 + \frac{1 - \pi}{(f_{\theta}(x_2) - c)^2} + \pi (f_{\theta}(x_2) - c)^2 + \frac{1 - \pi}{(f_{\theta}(x_1) - c)^2} \right]$$
(11)

$$= \sum_{i=1}^{2} \mathbb{E}_{x_{i} \sim P_{i}} \left[\pi (f_{\theta}(x_{i}) - c)^{2} + \frac{1 - \pi}{(f_{\theta}(x_{i}) - c)^{2}} \right]$$
(12)

$$\geq 2\sqrt{\pi(1-\pi)}\tag{13}$$

where $0.5 < \pi < 1$ implies the majority assumption and the equality holds when $(f_{\theta}(x_i) - c)^2 = \sqrt{(1-\pi)/\pi}$ for all i. All data points will be put at the hypersphere's surface centered around c with a radius $\sqrt{(1-\pi)/\pi}$ in the feature space when the model is optimized. However, the optimal loss has nothing to do with the model parameters, and the optimized model is unlikely to produce useful representations for zero-shot AD in the feature space.

On the other hand, if we apply batch normalization in the model f_{θ} , we won't have the optimal loss function irrelevant to the parameters. To see this, note that batch normalization will shift the data/feature vectors toward the origin. Thus x_1 in training task P_1^{π} and x_2 in training task P_2^{π} should have similar representations as they both take the majority in each task. Similarly, x_2 in task P_1^{π} and x_1 in task P_2^{π} are minorities, thus mapped far away from the origin in the feature space. Therefore, the symmetry breaks in Eq. (11) and the above optimal loss disappears.

C.2. Additional Results on CIFAR100-C

We test all methods on all corruption types of CIFAR100-C. The results are presented in Tab. 7.

Table 7. AUC (%) with standard deviation for anomaly detection on CIFAR-100-C (Hendrycks & Dietterich, 2019). For our method and OC-MAML, models are trained on all classes of the primitive CIFAR-100.

	ne primitive CI			100	2007
Noise Type	Method ACD DEVIDE	1%	5%	10%	20%
	ACR-DSVDD ACR-BCE	87.7±1.4 84.3±2.2	86.3±0.9 86.0±0.3	85.9±0.4 86.0±0.2	85.6±0.4 85.7±0.4
gaussian noise	Feat+BN + BN	62.5 ± 3.1	61.8±1.7	61.2±0.6	60.2±0.4
	OC-MAML (1-shot) CLIP-AD	53.0±3.6 82.3±1.1	54.1±1.9 82.6±0.9	55.8±0.6 82.3±0.9	57.1±1.0 82.6±0.1
	ACR-DSVDD ACR-BCE	85.5±1.6 87.1±2.4	86.5±0.2 86.3±0.6	87.3±0.6 86.8±0.5	86.4±0.4 86.4±0.1
shot noise	Feat+BN + BN	59.7±2.0	60.9±1.4	61.0 ± 0.6	60.1±0.6
	OC-MAML (1-shot)	53.8±4.7	52.8±1.1	53.6±1.0	53.8±1.3
	CLIP-AD	83.0±1.6	84.1±0.3	83.9±0.5	83.3±0.3
	ACR-DSVDD ACR-BCE	80.5±3.7 81.7±1.0	81.5±0.5 81.0±0.5	80.7±0.7 80.8±0.7	79.8±0.2 79.5±0.3
impulse noise	Feat+BN + BN	64.3±2.7	63.0±0.3	62.2±0.8	61.2±0.6
	OC-MAML (1-shot)	53.6±2.5	54.8 ± 1.6	53.6 ± 1.1	53.8±0.9
	CLIP-AD	81.5±2.0	82.7±0.4	82.3±0.5	82.2±0.2
	ACR-DSVDD	86.5±2.0	85.8±0.8	86.0±0.4	85.1±0.2
speckle noise	ACR-BCE Feat+BN + BN	85.9±1.7 61.8±2.8	86.4±0.4 61.0±1.0	85.7±0.6 61.0±0.9	85.4±0.4 59.8±0.3
	OC-MAML (1-shot)	52.2±2.7	52.8±1.2	53.5±1.2	53.7±0.4
	CLIP-AD	84.6±1.6	83.7±0.4	84.1±0.4	84.2±0.3
	ACR-DSVDD	88.5±1.1	88.5±0.7	88.7±0.4	88.6±0.3
gaussian blur	ACR-BCE	85.6±1.3	85.0 ± 0.6	85.0 ± 0.9	84.7±0.5
gaassan oran	Feat+BN + BN OC-MAML (1-shot)	64.9±1.5 55.6±3.6	65.3±1.2 56.6±0.6	64.0±0.9 56.8±1.1	62.7±0.4
	CLIP-AD	91.9±0.8	92.7±0.5	92.1±0.5	57.6±0.6 92.3±0.2
	ACR-DSVDD	89.7±1.8	89.5±0.8	89.1±0.3	89.2±0.3
defocue blur	ACR-BCE	86.5±1.3	86.5 ± 0.6	86.3±0.3	85.9±0.4
defocus blur	Feat+BN + BN	66.0 ± 1.8	65.4 ± 1.1	63.7±0.6	63.2±0.3
	OC-MAML (1-shot) CLIP-AD	53.5±2.5 93.1±1.4	51.7±1.7 92.9±0.3	54.0±1.8 92.8±0.3	54.7±0.7 92.8±0.2
.112	ACR-DSVDD ACR-BCE	87.0±2.1 85.4±1.0	87.9±0.4 86.1±0.4	87.7±0.4 86.4±0.4	87.6±0.2 86.1±0.3
glass blur	Feat+BN + BN	63.9 ± 2.2	63.0 ± 1.7	63.6 ± 0.5	62.2±0.4
	OC-MAML (1-shot) CLIP-AD	52.8±1.9 85.4±0.5	53.1±1.7 85.0±1.1	53.9±0.9 84.2±0.7	53.7±1.4 84.4±0.3
	ACR-DSVDD ACR-BCE	89.2±0.4 86.3±1.9	89.6±0.8 85.3±1.0	89.1±0.5 85.7±0.2	88.6±0.5 84.9±0.2
motion blur	Feat+BN + BN	66.6±3.1	64.8±1.2	63.4±0.6	62.4±0.3
	OC-MAML (1-shot)	50.5±3.1	52.3±1.6	53.1±0.9	53.6±0.7
	CLIP-AD	91.8±1.4	92.9±0.4	92.7±0.3	92.8±0.3
zoom blur	ACR-DSVDD	90.3±1.7	89.6±0.7	89.8±0.4	89.4±0.3
	ACR-BCE Feat+BN + BN	87.5±1.8 65.2±1.1	86.5±1.0 65.7±0.7	86.4±0.2 66.1±0.3	86.4±0.3 64.2±0.4
	OC-MAML (1-shot)	50.6±3.2	53.8 ± 0.8	53.7 ± 1.4	54.2±0.4
	CLIP-AD	94.2±1.4	94.4±0.3	94.3±0.3	93.9±0.3
snow	ACR-DSVDD	87.7±1.2	87.7±1.0	87.6±0.4	87.4±0.3
	ACR-BCE	84.4±2.6	85.5±0.8	85.5±0.6	84.4±0.0
	Feat+BN + BN OC-MAML (1-shot)	67.1±1.9 56.7±4.5	65.6±0.9 54.5±1.8	64.5±0.4 56.8±0.6	63.3±0.8 57.3±0.2
	CLIP-AD	91.7±0.8	92.9±0.4	93.3±0.2	93.2±0.2
	ACR-DSVDD	86.2±1.8	85.2±0.6	85.4±0.9	85.0±0.2
fog	ACR-BCE	78.8±2.7	77.7±0.5	77.3±0.7	77.2±0.6
<u> </u>	Feat+BN + BN OC-MAML (1-shot)	64.5±2.1 51.9±3.6	62.9±0.8 52.9±0.9	62.5±0.4 53.4±0.6	61.0±0.5 53.7±0.2
	CLIP-AD	91.9±0.8	92.3±0.5	92.2±0.4	92.3±0.3
	ACR-DSVDD	88.2±1.5	88.0±0.9	87.4±0.6	87.2±0.3
frost	ACR-BCE	83.2±1.4	84.1±1.2	84.6 ± 0.6	83.7±0.4
	Feat+BN + BN OC-MAML (1-shot)	63.0±1.0 52.8±1.3	63.2±0.5 52.4±2.0	62.7±1.3 53.6±0.7	61.7±0.3 53.2±1.1
	CLIP-AD	92.9±0.6	93.1±0.2	93.6±0.7	93.2±1.1
	ACR-DSVDD	90.0±1.5	89.5±0.9	89.6±0.4	89.9±0.2
brightness	ACR-BCE	86.7±1.3	87.8±0.7	87.1 ± 0.8	87.2±0.4
brightness	Feat+BN + BN	67.6±2.1	69.8±0.4	68.2 ± 1.0	67.0±0.5
	OC-MAML (1-shot) CLIP-AD	53.6±1.1 94.6±0.4	56.8±1.5 95.6±0.3	56.2±0.7 95.4±0.3	56.8±0.5 95.3±0.2
	ACR-DSVDD ACR-BCE	88.1±1.5 86.2±2.3	89.2±0.6 87.7±0.3	89.0±0.6 87.2±0.6	88.7±0.1 87.3±0.3
spatter	Feat+BN + BN	68.7 ± 1.7	67.6±0.9	66.0 ± 0.9	65.2±0.4
	OC-MAML (1-shot) CLIP-AD	53.6±2.7	55.6±1.1	56.1±0.7	53.6±1.5 95.0±0.3
		94.7±0.6	95.2±0.4	95.1±0.2	
	ACR-DSVDD ACR-BCE	88.1±2.1 86.8±2.0	87.1±0.7 86.1±0.8	87.1±0.5 86.0±0.6	85.8±0.4 85.3±0.3
saturate	Feat+BN + BN	67.7±1.8	67.7±1.4	67.4±0.8	65.9±0.3
	OC-MAML (1-shot)	55.6±2.4	53.5±0.9	55.1 ± 0.8	54.1±1.2
	CLIP-AD	94.7±0.8	94.7±0.2	95.0±0.1	95.1±0.2
	ACR-DSVDD	76.4±1.8	75.1±1.8	74.9±0.5	74.5±0.4
contrast	ACR-BCE Feat+BN + BN	67.6±2.0 61.3±0.9	66.7±0.8 61.3±1.2	67.8±0.7 60.2±0.5	66.9±0.3 59.3±0.5
	OC-MAML (1-shot)	54.6±3.7	54.0 ± 0.3	53.1 ± 1.2	54.1±1.0
	CLIP-AD	89.3±1.8	88.9±0.5	88.3±0.4	88.8±0.2
	ACR-DSVDD	90.8±1.9	89.3±0.7	90.0±0.4	89.3±0.3
elastic transform	ACR-BCE Feat+BN + BN	87.6±1.0 65.6±2.3	86.7±0.8 65.2±0.6	87.4±0.6 63.9±0.7	87.2±0.4 62.0±0.3
canoue transfollil	OC-MAML (1-shot)	52.5±3.9	54.3±1.2	54.4±1.2	54.7±0.8
		89.1±1.1	90.0±0.3	89.4±0.5	89.4±0.3
	CLIP-AD		_	000.00	90.7±0.2
	ACR-DSVDD	91.7±0.5	91.1±0.6	90.8±0.6	90.7±0.2
pixelate	ACR-DSVDD Feat+BN + BN	66.4±1.5	65.6 ± 0.6	64.9 ± 0.6	63.8±0.3
pixelate	ACR-DSVDD Feat+BN + BN ACR-BCE	66.4±1.5 89.6±1.9	65.6±0.6 89.9±0.6	64.9±0.6 89.7±0.1	63.8±0.3 89.8±0.3
pixelate	ACR-DSVDD Feat+BN + BN	66.4±1.5	65.6 ± 0.6	64.9 ± 0.6	63.8±0.3
pixelate	ACR-DSVDD Feat+BN + BN ACR-BCE OC-MAML (1-shot) CLIP-AD	66.4±1.5 89.6±1.9 56.4±3.8 86.7±0.3	65.6±0.6 89.9±0.6 55.8±0.9 86.7±0.7	64.9±0.6 89.7±0.1 56.4±0.7 86.9±0.3	63.8±0.3 89.8±0.3 57.0±0.9 86.7±0.3
-	ACR-DSVDD Feat+BN + BN ACR-BCE OC-MAML (1-shot) CLIP-AD ACR-DSVDD ACR-BCE	66.4±1.5 89.6±1.9 56.4±3.8 86.7±0.3 89.8±1.4 89.1±1.2	65.6±0.6 89.9±0.6 55.8±0.9 86.7±0.7 91.0±0.5 88.8±0.8	64.9±0.6 89.7±0.1 56.4±0.7 86.9±0.3 90.5±0.7 89.1±0.5	63.8±0.3 89.8±0.3 57.0±0.9 86.7±0.3 90.4±0.3 88.6±0.3
pixelate jpeg compression	ACR-DSVDD Feat+BN + BN ACR-BCE OC-MAML (1-shot) CLIP-AD ACR-DSVDD	66.4±1.5 89.6±1.9 56.4±3.8 86.7±0.3	65.6±0.6 89.9±0.6 55.8±0.9 86.7±0.7 91.0±0.5	64.9±0.6 89.7±0.1 56.4±0.7 86.9±0.3	63.8±0.3 89.8±0.3 57.0±0.9 86.7±0.3